JACS
JOURNAL OF THE AMERICAN CHEMICAL SOCIETY
Communication
pubs.acs.org/JACS

Stepwise Pore Size Reduction of Ordered Nanoporous Silica Materials at Angstrom Precision

Siddharth Jambhrunkar,[†] Meihua Yu,[†] Jie Yang,[†] Jun Zhang,[†] Abhijit Shrotri,[†] Liliana Endo-Munoz,[‡] Joël Moreau,[§] Gaoqing Lu,[†] and Chengzhong Yu*,[†]

[†]ARC Centre of Excellence for Functional Nanomaterials and Australian Institute for Bioengineering and Nanotechnology, The University of Queensland, Brisbane, QLD 4072, Australia

[‡]Diamantina Institute, Princess Alexandra Hospital, Ipswich Road, Brisbane, QLD 4102, Australia

[§]Ecole Nationale Supérieure de Chimie de Montpellier, 34296 Montpellier CEDEX 5, France

Supporting Information

ABSTRACT: A facile vacuum-assisted vapor deposition process has been developed to control the pore size of ordered mesoporous silica materials in a stepwise manner with angstrom precision, providing an unprecedented paradigm for screening a designer hydrophobic drug nanocarrier with optimized pore diameter to maximize drug solubility.

Since the discovery of MCM-41[1] and SBA-15,[2] ordered mesoporous silica materials have attracted ever-increasing attention because of their potential applications in many fields.[3] The uniform mesopores and adjustable pore sizes are important characteristics of mesoporous materials that are critically important for the controlled immobilization and release behavior of guest molecules,[4] catalytic reaction performance in confined nanospaces,[5] controlled release of hydrophobic drugs,[4,6] and use as nanocarriers for water-insoluble drugs.[7] To date, much effort has been devoted to controlling the pore size of ordered mesoporous silica materials. Generally, the pore size can be increased using post-synthesis methods or the addition of swelling agents[2] or by varying the structure-directing template.[8] Alternatively, the pore size can be reduced by the grafting method,[9] metal−organic chemical vapor deposition,[10] or atomic layer deposition (ALD).[11] Of these, ALD has been widely used to modify mesoporous silica materials with another oxide phase (e.g., TiO_2, HfO_2),[11b−d] showing pore size reduction at the atomic scale. However, it is difficult to achieve a constant pore size reduction in each cycle. Moreover, unlike zeolites or metal−organic frameworks, whose pore sizes can be designed at angstrom precision for size-selective applications,[12] it has been a big challenge to achieve such precise control over the pore sizes of ordered mesoporous silica materials since their discovery, especially over a wide mesopore size range and in a reproducible manner.

Up to 40% of new chemical drugs emerging from high-throughput screening processes are poorly water-soluble, posing the challenge of improving their solubility and hence their bioavailability.[13] Various approaches to address this issue have been studied,[14] among which reducing the hydrophobic drug particle size[15] is an efficient one, as reflected by the Ostwald−Freundlich equation.[16] However, methods of reducing drug particle sizes find limitations in downsizing drug particle sizes below 20 nm, a regime in which a dramatic increase in solubility is expected. Ordered mesoporous silica materials provide an adjustable confined nanospace, and hence, the size of the drug loaded inside can be limited. By confining the hydrophobic drug indole-3-butyric acid into MCM-41 with a pore size of 3.31 nm, its solubility was increased ca. 2-fold relative to the drug alone.[7c] Surprisingly, this is a rare case showing the influence of nanoconfinement on the solubility of drugs. It is not known whether this concept can be generally applied to other hydrophobic drugs. Importantly, to our knowledge, the relationship between the pore size of the host mesoporous material and the solubility of the loaded drug has not been reported. We hypothesized that there exists an optimized pore size displaying the highest solubility for a given hydrophobic drug [see Influence of Pore Size on Solubility in the Supporting Information (SI)]. To test this hypothesis, it was necessary to design a series of mesoporous silica materials with precisely controlled pore sizes and encapsulate the drug in them.

Herein we report a facile vacuum-assisted vapor deposition (VVD) approach for reducing the pore size of ordered mesoporous silica materials in a stepwise and precise fashion (Figure 1). The step size was adjustable in increments of 0.29 ± 0.06 nm using tetraethoxyorthosilicate (TEOS) or 0.54 ± 0.06 nm using tetramethoxyorthosilicate (TMOS) as the silica precursor. A surface-chemistry switching mechanism is proposed (Figure 1A). By means of the surface silanols at the pore surface, the TEOS or TMOS vapor molecules are anchored on the pore surface by VVD (step I), which is followed by calcination (step II) to complete one cycle. Upon completion of one cycle, the pore diameter is reduced, and the silanols are regenerated and can be used for a subsequent cycle. This approach was tested using two ordered mesoporous silica materials with different initial pore sizes, SBA-15[2] and MCM-41[1] (Figure 1B). In consecutive cycles, the pore size reduction was consistent for both materials and/or silica precursors. By encapsulation of the hydrophobic drug curcumin in the series of MCM-41 materials with controlled pore sizes, a pore size−solubility function was obtained that shows an optimal pore size

Received: March 9, 2013
Published: May 13, 2013

   dx.doi.org/10.1021/ja402463h | J. Am. Chem. Soc. 2013, 135, 8444−8447

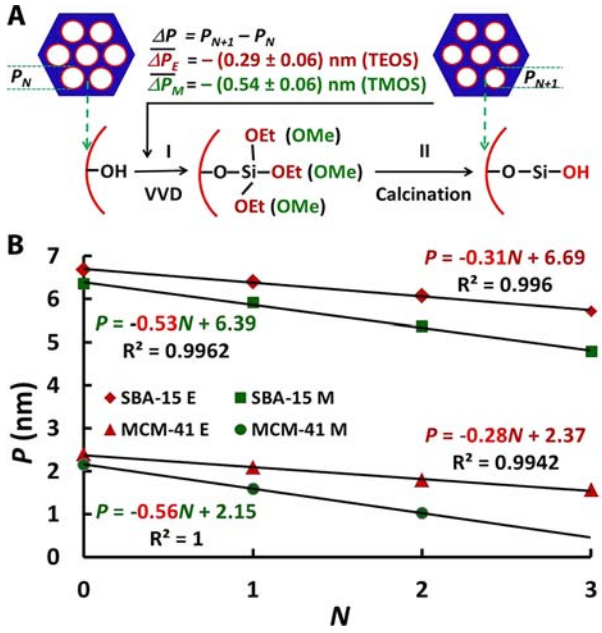

Figure 1. (A) Scheme demonstrating the VVD approach for stepwise reduction of the pore sizes of ordered mesoporous silica materials over a precise range using TEOS or TMOS (abbreviated as "E" or "M", respectively). N is the cycle number, and P_N and P_{N+1} are the pore diameters before and after cycle N, respectively. ΔP denotes the pore size change after one VVD cycle. $\overline{\Delta P}$ denotes the mean pore size reduction and is expressed as the mean ± standard deviation after three cycles, except for MCM-41 with TMOS, where only two cycles were included in the linear regression. (B) Variation of the pore diameter, P, as a function of N for both SBA-15 and MCM-41 materials. R^2 is the regression coefficient.

(1.70 nm) where curcumin possesses the highest solubility (4.5 times higher than for the drug alone).

SBA-15 and MCM-41 were prepared according to published methods[17] with slight variations (see the Experimental Section in the SI). To adjust the pore size, 0.8 g of calcined SBA-15 or MCM-41 material was placed in a home-designed VVD apparatus to undergo the VVD process (Figure S1 in the SI). The VVD process was performed by exposure of the mesoporous silica material to either TEOS or TMOS for 24 h at 60 °C (step I) followed by calcination (step II) (Figure 1A). The samples obtained in one VVD cycle are denoted as sample-DN-E/M and sample-CN-E/M, where "sample" is SBA-15 or MCM-41, "D" refers to the deposition step, and "C" refers to the calcination step (N, E, and M are defined in Figure 1).

The X-ray diffraction (XRD) patterns of SBA-15-CN-E (N = 0−3) are shown in Figure S2A. For SBA-15-C0-E before VVD treatment, three well-resolved diffractions appear at 2θ = 0.90, 1.56, and 1.81° with a reciprocal d-spacing ratio close to $1:\sqrt{3}:2$, which can be indexed as the 100, 110, and 200 reflections of an ordered two-dimensional hexagonal mesostructure ($p6mm$). From the intense (100) peak, a d_{100} spacing of 9.81 nm was calculated, corresponding to a unit cell parameter (a) of 11.33 nm (Table S1 in the SI). The XRD patterns for SBA-15-CN-E after successive VVD cycles (N = 1−3) are similar to that of SBA-15-C0-E, demonstrating retention of the ordered hexagonal mesostructure. Moreover, the positions of the three diffractions are similar for the four materials. In addition, a gradual increase in the ratio of intensity of 200 to 110 peaks can be observed, suggesting a slight increase in wall thickness in each VVD cycle.[18]

The N_2 adsorption−desorption isotherms for SBA-15-CN-E (N = 0−3) are typical type-IV isotherms with a steep capillary condensation step occurring at a relative pressure (P/P_0) range of 0.7−0.8, characteristic of ordered mesoporous materials with large and uniform mesopores (Figure S3A). The pore size variation in SBA-15-CN-E can be clearly seen in their pore size distribution curves calculated from the adsorption branch using the Barrett−Joyner−Halenda (BJH) model after Gaussian fitting (Figure S2B). The pore sizes were calculated to be 6.67, 6.40, 6.07, and 5.71 nm for N = 0−3, respectively, and the pore size distribution curve was narrow even after three VVD cycles. After linear regression analysis, the equation $P = -0.31N + 6.69$) with a regression coefficient of R^2 = 0.9960 was obtained (Figure 1B), indicating a high statistical significance of the VVD process to achieve fine control over the pore size. The pore sizes as well as surface areas and pore volumes of SBA-15-CN-E (N = 0−3) are summarized in Table S1 for comparison.

To understand why the pore size was precisely reduced after every cycle in the VVD process in a stepwise manner, Fourier transform IR (FTIR) analysis of the SBA-15 material treated in each step of the three cycles was performed. To show the surface chemistry changes clearly, only regions of interest are displayed in Figure 2. Before the VVD process, SBA-15-C0-E exhibited one peak at 3745 cm^{-1} (Figure 2A) assigned to

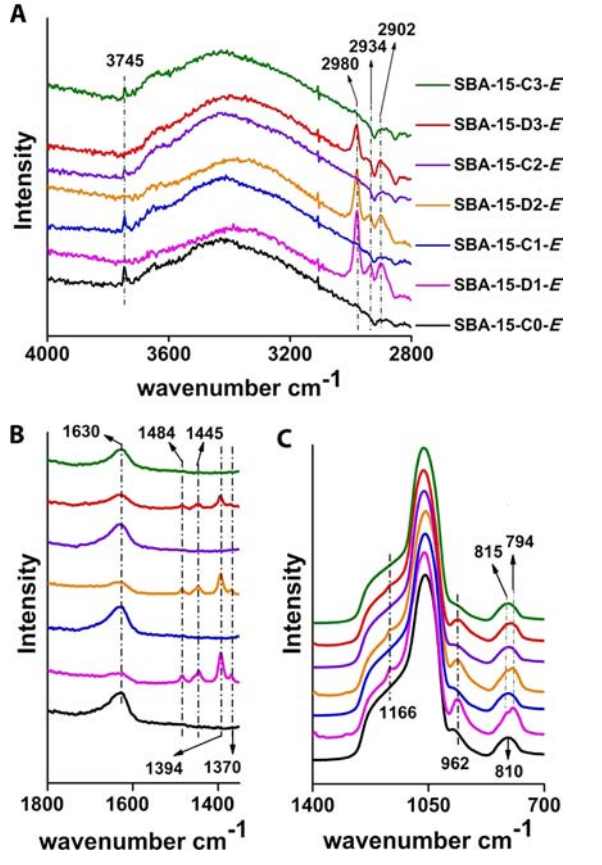

Figure 2. FTIR spectra of the SBA-15 sample before, during, and after treatment with the VVD process for three cycles using TEOS as the silica precursor. Samples are named as SBA-15-DN-E and SBA-15-CN-E, where D denotes the deposited sample after step I in the cycle, C denotes the calcined sample after step II in the cycle, N denotes the cycle number, and E denotes TEOS.

dx.doi.org/10.1021/ja402463h | J. Am. Chem. Soc. 2013, 135, 8444−8447

isolated silanols [ν(O−H)].[19] After the first deposition step (SBA-15-D1-E), this peak could not be observed. Instead, a group of peaks at 2902, 2934, and 2980 cm^{-1} appeared, which can be assigned to ν(C−H) of unhydrolyzed ethoxy groups ($Si-OCH_2CH_3$).[19c] After the first calcination step (SBA-15-C1-E), the peaks assigned to ethoxy groups disappeared, and the peak at 3745 cm^{-1} associated with surface silanols was regenerated. The above results indicate that in one VVD cycle, the surface silanols are "switched off" and ethoxy groups are "switched on" in the deposition step and then the silanols are "switched on" and the ethoxy groups are "switched off" in the calcination step (see Figure 1A). Moreover, the "on/off" surface chemistry was repeatedly observed over three consecutive cycles.

The surface chemistry switching mechanism was further confirmed by the spectra shown in Figure 2B,C. The bands associated with ethoxy groups at 1166 [$\rho(CH_3)$], 1370 [$\omega(CH_2)$], 1394 [$\delta_s(CH_3)$], 1445 [$\delta'_a(CH_2)$] and 1484 cm^{-1} [$\delta_a(CH_3) + \delta_a(CH_2)$] were observed only after each deposition step. The band at 962 cm^{-1} (Figure 2C) is the characteristic peak for $\rho(CH_3)$, which overlaps with the band of silanols (observed after calcination) with relatively weaker intensity.[20] The band observed at 810 cm^{-1} after each calcination step (Figure 2C) can be indexed to symmetric Si−O−Si stretching [ν_s(Si−O−Si)].[19a] After deposition, only two peaks at 794 [ν(Si−O)] and 815 cm^{-1} [δs(Si−O−C)] indexed to the nonreacted ($Si-OCH_2CH_3$) groups were observed.[21] The intensity of the band associated with physiosorbed water at 1630 cm^{-1} was higher when Si−OH was "switched on" and lower when Si−OH was "switched off", consistent with the hydrophilicity/hydrophobicity change of the pore walls and the surface chemistry switching mechanism.

The VVD process was further applied to MCM-41 materials using TEOS as the silica precursor. Both XRD and nitrogen sorption results showed that the ordered hexagonal mesostructure with narrow pore size distribution was retained after three VVD cycles (Figures S3 and S4). FTIR spectra (Figure S5) demonstrated the mechanism proposed in Figure 1 to be reproducible for both SBA-15 and MCM-41 materials. After linear regression, the equation $P = -0.28N + 2.37$ with $R^2 = 0.9942$ was obtained (Figure 1B), confirming that our VVD process can be applied to both SBA-15 and MCM-41 to achieve a stepwise pore size reduction in a precise range of 0.29 ± 0.06 nm per step. The VVD process was repeated on freshly synthesized SBA-15 and MCM-41, further demonstrating its reproducibility (see Reproducibility of VVD process in the SI along with Figures S6−S8 and Table S2).

The VVD process was further conducted on SBA-15 and MCM-41 materials using TMOS as the silica precursor. The XRD patterns for SBA-15-C*N*-M (Figure S9A) and MCM-41-C*N*-M (Figure S10A) showed that the ordered hexagonal structure was retained after each VVD cycle. N_2 adsorption−desorption isotherms for SBA-15-C*N*-M (N = 0−3) and MCM-41-C*N*-M (N = 0−2) (Figure S11) were typical type-IV isotherms, similar to those obtained for SBA-15-C*N*-E (N = 0−3) and MCM-41-C*N*-E (N = 0−3). The pore sizes, surface areas, and pore volumes of SBA-15-C*N*-M (N = 0−3) and MCM-41-C*N*-M (N = 0−2) are summarized in Table S1. For MCM-41-C3-M, the mesopores were nearly blocked, and it was very difficult to detect the pore size using the BJH model because the pore size was in microporous range. Hence, the pore size distribution curve for MCM-41 material was calculated for only two VVD cycles.

The pore size distribution data for SBA-15-C*N*-M (N = 0−3) and MCM-41-C*N*-M (N = 0−2) are shown in Figures S9B and S10B, respectively. After linear regression analysis, the equations $P = -0.53N + 6.39$ ($R^2 = 0.9962$) and $P = -0.56N + 2.15$ ($R^2 = 1$) were obtained for the SBA-15 and MCM-41 groups, respectively, indicating high statistical significance (Figure 1B). Using TMOS in the VVD process led to a stepwise pore size reduction of 0.54 ± 0.06 nm per step for SBA-15 and MCM-41. FTIR analysis was performed for SBA-15-C*N*-M and MCM-41-C*N*-M, and surface chemistry "on/off" switching similar to that for SBA-15-C*N*-E and MCM-41-C*N*-E was observed (Figures S12 and S13).

To understand the difference in the pore size reduction steps using TEOS (0.29 ± 0.06 nm) and TMOS (0.54 ± 0.06 nm) in our VVD process, the weight change upon deposition (step I) was carefully monitored for SBA-15 using TEOS as the silica precursor. The weight gains observed for SBA-15-D*N*-E (N = 1−3) are listed in Table S3. After each deposition step, the number of TEOS molecules deposited on the internal surface of SBA-15 had a constant value of 0.9 nm^{-2}. Because TEOS has a molecular size of 0.93 nm,[22] the surface coverage constant of 0.9 nm^{-2} is consistent with monolayer-like deposition behavior on the wall surface (Figure S14A). After calcination (step II) to convert $-Si(OEt)_3$ to Si−OH, the newly generated Si−OH must be distributed sparsely because of its smaller size compared with $-Si(OEt)_3$. It is noted that a densely packed Si−OH monolayer theoretically would generate a pore size reduction of 0.62 nm (Figure S14C). The sparse distribution of Si−OH in our model (Figure S14B) leads to the observed pore size reduction of 0.29 ± 0.06 nm. Because TMOS molecules are smaller than TEOS molecules, the number of TMOS molecules deposited on the internal surface of SBA-15 during step I should be higher (Figure S14A), leading to relatively higher density of newly generated Si−OH after step II, which results in a larger pore size reduction step of 0.54 ± 0.06 nm.

Finally, the series of MCM-41 nanoporous materials with precisely controlled pore sizes were utilized to confine the hydrophobic drug curcumin in order to study the pore size−solubility relationship. As shown in Figure 3, pure curcumin has a very low water solubility of 0.31 μg/mL. Curcumin encapsulated in pristine MCM-41 with a pore size of 2.22 nm had an improved solubility of 0.53 μg/mL. The curcumin solubility further increased with decreasing pore size, reaching a

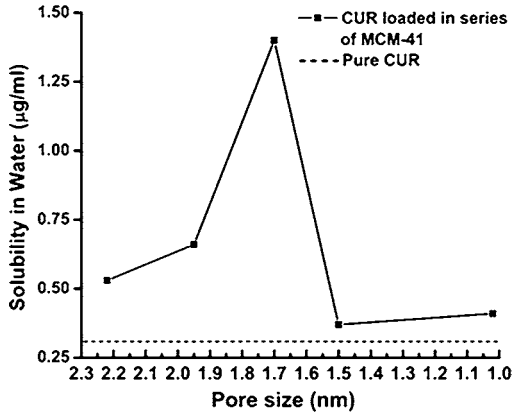

Figure 3. Correlation between pore size and curcumin solubility in water after loading of curcumin into a series of calcined MCM-41 materials with precisely controlled pore sizes.

maximum of 1.40 μg/mL (4.5 times of pure curcumin) at the optimal pore size of 1.70 nm. However, the curcumin solubility diminished significantly when the pore size was further decreased from 1.70 to 1.50 and 1.02 nm. Our experimental observations are in good accordance with the theoretical predictions (see the SI).

In conclusion, we have developed a novel VVD approach to achieve stepwise reductions in the pore size of mesoporous silica materials at angstrom precision. The pore size−solubility relationship has been established, allowing a mesoporous material with an optimized pore size displaying maximized drug solubility to be identified. With our discovery, the pore sizes of ordered mesoporous materials can be adjusted over a broad regime with a precision that has not been achieved before, offering new materials for advanced pore-size-dependent applications.

■ ASSOCIATED CONTENT

Ⓢ Supporting Information

Experimental methods and other characterizations. This material is available free of charge via the Internet at http://pubs.acs.org.

■ AUTHOR INFORMATION

Corresponding Author

c.yu@uq.edu.au

Notes

The authors declare no competing financial interest.

■ ACKNOWLEDGMENTS

This work was supported by the Australian Research Council.

■ REFERENCES

(1) Kresge, C. T.; Leonowicz, M. E.; Roth, W. J.; Vartuli, J. C.; Beck, J. S. *Nature* **1992**, *359*, 710.

(2) Zhao, D. Y.; Feng, J. L.; Huo, Q. S.; Melosh, N.; Fredrickson, G. H.; Chmelka, B. F.; Stucky, G. D. *Science* **1998**, *279*, 548.

(3) (a) Vallet-Regi, M.; Balas, F.; Arcos, D. *Angew. Chem., Int. Ed.* **2007**, *46*, 7548. (b) Somorjai, G. A.; Frei, H.; Park, J. Y. *J. Am. Chem. Soc.* **2009**, *131*, 16589.

(4) Balas, F.; Manzano, M.; Horcajada, P.; Vallet-Regi, M. *J. Am. Chem. Soc.* **2006**, *128*, 8116.

(5) (a) Ying, J. Y.; Mehnert, C. P.; Wong, M. S. *Angew. Chem., Int. Ed.* **1999**, *38*, 56. (b) Nandi, M.; Mondal, J.; Sarkar, K.; Yamauchi, Y.; Bhaumik, A. *Chem. Commun.* **2011**, *47*, 6677.

(6) Mellaerts, R.; Jammaer, J. A. G.; Van Speybroeck, M.; Chen, H.; Van Humbeeck, J.; Augustijns, P.; Van den Mooter, G.; Martens, J. A. *Langmuir* **2008**, *24*, 8651.

(7) (a) Lu, J.; Liong, M.; Zink, J. I.; Tamanoi, F. *Small* **2007**, *3*, 1341. (b) Lu, J.; Liong, M.; Li, Z. X.; Zink, J. I.; Tamanoi, F. *Small* **2010**, *6*, 1794. (c) Ambrogi, V.; Famiani, F.; Perioli, L.; Marmottini, F.; Di Cunzolo, I.; Rossi, C. *Microporous Mesoporous Mater.* **2006**, *96*, 177.

(8) Yu, C. Z.; Fan, J.; Tian, B. Z.; Stucky, G. D.; Zhao, D. Y. *J. Phys. Chem. B* **2003**, *107*, 13368.

(9) Zhao, X. S.; Lu, G. Q. M.; Hu, X. *Chem. Commun.* **1999**, 1391.

(10) Zhang, Y.; Lam, F. L. Y.; Hu, X. J.; Yan, Z. F. *Chem. Commun.* **2008**, 5131.

(11) (a) Berland, B. S.; Gartland, I. P.; Ott, A. W.; George, S. M. *Chem. Mater.* **1998**, *10*, 3941. (b) Mahurin, S.; Bao, L.; Yan, W.; Liang, C.; Dai, S. *J. Non-Cryst. Solids* **2006**, *352*, 3280. (c) Pagan-Torres, Y. J.; Gallo, J. M. R.; Wang, D.; Pham, H. N.; Libera, J. A.; Marshall, C. L.; Elam, J. W.; Datye, A. K.; Dumesic, J. A. *ACS Catal.* **2011**, *1*, 1234. (d) Dendooven, J.; Goris, B.; Devloo-Casier, K.; Levrau, E.; Biermans, E.; Baklanov, M. R.; Ludwig, K. F.; Van der Voort, P.; Bals, S.; Detavernier, C. *Chem. Mater.* **2012**, *24*, 1992.

(12) Li, J. R.; Kuppler, R. J.; Zhou, H. C. *Chem. Soc. Rev.* **2009**, *38*, 1477.

(13) Lipinski, C. *Am. Pharm. Rev.* **2002**, *5*, 82.

(14) Chadha, R.; Kapoor, V. K.; Thakur, D.; Kaur, R.; Arora, P.; Jain, D. V. S. *J. Sci. Ind. Res.* **2008**, *67*, 185.

(15) Rabinow, B. E. *Nat. Rev. Drug Discovery* **2004**, *3*, 785.

(16) Ostwald, W. *Z. Phys. Chem., Stoechiom. Verwandtschaftsl.* **1900**, *34*, 495.

(17) (a) Pan, D. H.; Yuan, P.; Zhao, L. Z.; Liu, N. A.; Zhou, L.; Wei, G. F.; Zhang, J.; Ling, Y. C.; Fan, Y.; Wei, B. Y.; Liu, H. Y.; Yu, C. Z.; Bao, X. J. *Chem. Mater.* **2009**, *21*, 5413. (b) Yang, S.; Zhao, L. Z.; Yu, C. Z.; Zhou, X. F.; Tang, J. W.; Yuan, P.; Chen, D. Y.; Zhao, D. Y. *J. Am. Chem. Soc.* **2006**, *128*, 10460.

(18) Kozlova, S. A.; Kirik, S. D. *Microporous Mesoporous Mater.* **2010**, *133*, 124.

(19) (a) Muroya, M. *Colloids Surf., A* **1999**, *157*, 147. (b) Pan, D. H.; Zhao, L. Z.; Qian, K.; Tan, L.; Zhou, L.; Zhang, J.; Huang, X. D.; Fan, Y.; Liu, H. Y.; Yu, C. Z.; Bao, X. J. *J. Mater. Res.* **2011**, *26*, 804. (c) Tejedor-Tejedor, M. I.; Paredes, L.; Anderson, M. A. *Chem. Mater.* **1998**, *10*, 3410.

(20) Zhang, J.; Yu, M. H.; Yuan, P.; Wang, H. N.; Qian, K.; Tan, L.; Wang, Y. H.; Yu, C. Z. *J. Mater. Res.* **2010**, *25*, 648.

(21) (a) Velasco-Santos, C.; Martinez-Hernandez, A. L.; Brostow, W.; Castaño, V. M. *J. Nanomater.* **2011**, No. 928659. (b) Bourgeat-Lami, E.; Tissot, I.; Lefebvre, F. *Macromolecules* **2002**, *35*, 6185.

(22) Wróbel, A. M.; Walkiewicz-Pietrzykowska, A.; Stasiak, M.; Kulpiúski, J. *Chem. Vap. Deposition* **1996**, *2*, 285.